Arch. Min. Sci. **66** (2021), 3, 369-384

Electronic version (in color) of this paper is available: http://mining.archives.pl

DOI 10.24425/ams.2021.138594

NGUYEN QUOC LONG[1*], ROPESH GOYAL[2], LUYEN K. BUI[1], CAO XUAN CUONG[1], LE VAN CANH[1], NGUYEN QUANG MINH[1], XUAN-NAM BUI[3]

Optimal Choice of the Number of Ground Control Points for Developing Precise DSM Using Light-Weight UAV in Small and Medium-Sized Open-Pit Mine

UAV technology is being applied for DSM generation in open-pit mines with a well-established fact that the precision of such DSM is improved by increasing the number of Ground Control Points (GCPs). However, DSMs are updated frequently in an open-pit mine where the surface is excavated continuously. This imposes a challenge to arrange and maintain the GCPs in the field. Therefore, an optimal number of GCPs should be determined to obtain sufficiently accurate DSMs while maintaining safety, time, and cost-effectiveness in the project. This study investigates the influence of the numbers of GCPs and their network configuration in the Long Son quarry, Vietnam. The analysis involved DSMs generated from eight cases with a total of 18 GCPs and each having five network configurations. The inter-case and intra-case accuracy of DSMs is assessed based on $RMSE_{XY}$, $RMSE_{Z}$, and $RMSE_{XYZ}$. The results show that for a small- or medium-sized open-pit mine having an area of approximately 36 hectares, five GCPs are sufficient to achieve an overall accuracy of less than 10 cm. It is further shown that the optimal choice of the number of GCPs for DSM generation in such a mining site is seven due to a significant improvement in accuracy (<3.5 cm) and a decrease in configuration dependency compared to the five GCPs.

Keywords: Lightweight UAV, Digital Surface Model, Ground Control Points, Small and Medium-Sized Open-pit Mine

[1] HANOI UNIVERSITY OF MINING AND GEOLOGY, FACULTY OF GEOMATICS AND LAND ADMINISTRATION, 18 VIEN STREET, HANOI, 10000, VIETNAM

[2] INDIAN INSTITUTE OF TECHNOLOGY KANPUR, DEPARTMENT OF CIVIL ENGINEERING, KANPUR-208016, UTTAR PRADESH, INDIA

[3] HANOI UNIVERSITY OF MINING AND GEOLOGY, FACULTY OF MINING, 18 VIEN STREET, HANOI, 10000, VIETNAM

* Corresponding author: nguyenquoclong@humg.edu.vn

1. Introduction

Small and medium-sized open-pit mines such as quarries are often located in areas with complicated terrains and various geological conditions. Many of them are high limestone mountains with significant changes in terrain elevation, while others are at the height of 100 m below sea level. These lead to challenges for ground surveying when using the traditional methods because of the limited accessibility in the mining area or even inaccessibility in some extreme cases.

The rapid development of Unmanned Aerial Vehicle (UAV) technologies has brought many benefits to the mining industry in terms of safety, precision, and productivity. Recently, UAVs have been used extensively in open-pit mining areas for numerous applications such as pit and dump management [12], stockpile management [27], mapping of inaccessible steep inclines and cliffs [10], monitoring the dust particles [20], assessment of slope stability and mine subsidence [17], monitoring and analysing subsurface heating [11], geological modelling [15] along with other applications involving assets and infrastructure management/inspections and as-built versus as-designed comparisons. A detailed overview of the possible applications in the open-pit mining industry using different sensors attached to the UAVs is well documented in Ren et al. [30].

Most of the applications mentioned above require a precise high-resolution Digital Surface Model (DSM). There have been several studies on the generation of DSMs using UAVs for mining sites (e.g., [1,2,4,6,8,9,15,18,21,22,25]). Open-pit mining involves continuous excavation over time, and hence, surveying needs to be done at regular intervals. UAV-based surveying alone is not advantageous until it is attached to precise ground control points (GCPs). This is because the in-built GNSS in low-cost and lightweight UAVs do not meet the accuracy requirement. Canh et al. [19] have shown that with direct georeferencing of image data captured using lightweight UAV with onboard RTK positioning (DJI Phantom 4 RTK), it is not possible to obtain even the decimeter-level accurate DSM in complex mining terrains, such as ours. Some studies have also suggested the use of a few GCPs to achieve a certain accuracy level as compared to GCP based georeferencing or indirect georeferencing, and more importantly, to prevent the biases in focal length within the self-camera-calibration technique [3,9,26]. However, obtaining the vertical accuracy well within 5 cm with the direct georeferencing in lightweight UAVs is still challenging, especially for the open-pit mines. Thus, it becomes inevitable for indirect georeferencing of the collected UAV data sets using precise GCPs acquired with a dual-frequency GNSS receiver.

The accuracy achieved in the indirect georeferencing is dependent on the characteristics of GCPs, including the measurement precision and the distribution (i.e., the number of points and their spatial distribution) [23,24]. It is a well-established fact that a higher number of uniformly distributed GCPs will reduce the errors in georeferencing and thus increase the accuracy of the generated DSM [24]. However, one of the most important factors of introducing the UAV to the mining sector was to reduce the cost and increase productivity and safety. This aims to choose the optimal number of required GCPs, that is, the minimal sufficient in number and convenient to be organised in the field (their distribution), for our case, an open-pit mine.

There have been several studies to analyse the effect of the number and distribution of GCPs to construct a precise DSM (e.g., [5,7,14,16,28,29]). However, only a few studies have been applied to open-pit mines and relatively less for small to medium-sized open-pit mines. It becomes challenging, especially for small to medium-sized open-pit mines, because of the smaller site area and large undulations/depths. Shahbazi et al. [22] analysed the number and distribution of GCPs for DSM generation in an open-pit mine using a UAV. They conducted experiments with

six different sets, of which only one set consists of 22 GCPs, and all others have 3 GCPs. The authors recommended using a large number of well-distributed GCPs to achieve the highest precision. Villanueva and Blanco [13] used four different distribution patterns of data sets that consist of 4, 6, 8, 12, 16, and 20 GCPs to analyse the effect of the number and distribution of GCPs for the stockpile measurement. No other study in the literature were found by the authors discussing in detail the effect of the number and distribution of GCPs in DSM construction of small to medium-sized open-pit mines using lightweight UAVs.

In this paper, through rigorous experiments, we focus on delivering a detailed discussion on the optimal choice of the number of GCPs to achieve the most precise DSM in small to medium-sized open-pit mines. This is optimised in a way that fewer GCPs are required, and their stable monumentation can be easily arranged. This study is essential because of the similar mining practised in several parts of the world and extensively in Vietnam. The study focuses on the Long Son quarry that is of a typical configuration in its size, height difference, and surface roughness. Therefore, the results investigated from this study can be of assistance in designing networks of GCPs used for UAV-based topographical mapping in similar small- or medium-sized quarries in Vietnam.

2. Study area and materials

2.1. Study area

In this study, the experiments are conducted in the Long Son limestone quarry located in Thanh Hoa province in northern Vietnam, between latitudes 20°04′00″N and 20°05′30″N and longitudes 105°55′15″E and 105°56′00″E (Fig. 1). The total area of the mine is approximately 1.0 km^2, with an exploitation reserve of 4.0 million tons per year. Like many other quarries in Vietnam, the topographical characteristics of this quarry include benches, the toe of the benches, and steep slopes. At the time of the study, the mine was at the excavating level of 110 m. The maximum terrain difference is about 112 m, the average height of benches is 41 m, and the steepest slope is approximately 88˚.

2.2. Data collection

A DJI Phantom 4 Pro equipping with a 20-megapixel red, green, and blue camera and a GNSS/IMU is employed for the UAV survey. The camera's focal length is 8.8 mm, and the size of the sensor is 13.2 mm width by 8.8 mm height (https://www.dxomark.com). The UAV is a commercial lightweight quadcopter with manual or automatic flight modes set in Android or IOS smartphone applications. In this study, Pix4Dcapture installed on an iPhone 7 plus is used for flight planning. In the automatic mode, several important parameters are uploaded to the UAV, including a mapping area of 36 hectares, a flight height of 200 m above the ground, and an image forward, and a side-overlap of 80%. Also, a GNSS/IMU mounted on the UAV allows positioning of each camera with an average precision of 2.5 m. The positioning information of the cameras is stored in files of each image that is used for processing imagery to obtain photogrammetric products. The imagery acquisition was completed with 80 photos with the ground sample distances (GSD) ranging between 4.66 and 7.58 cm/pixel.

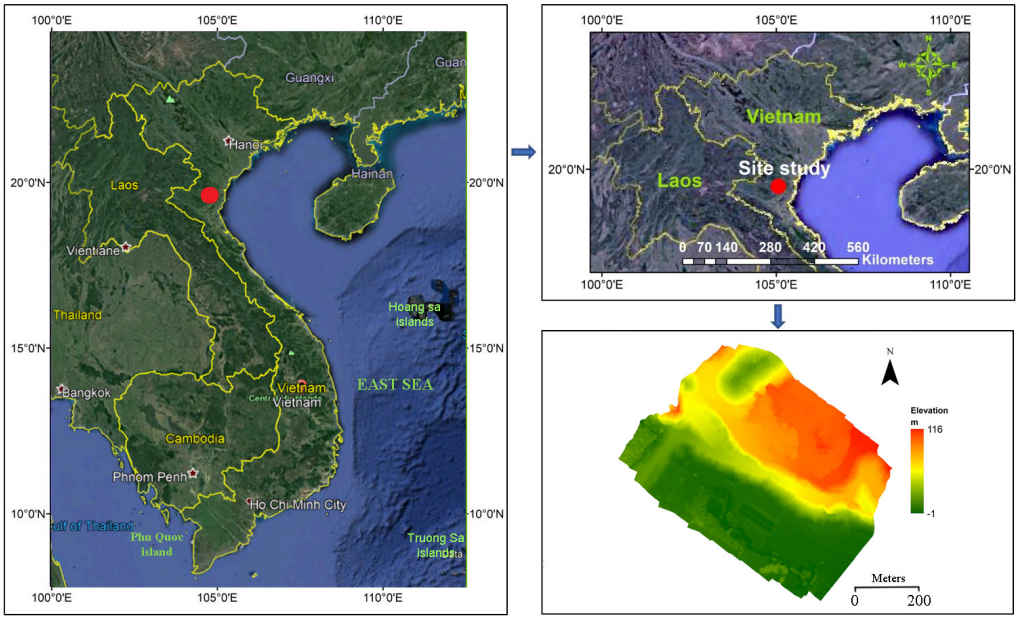

Fig. 1. Location and Digital Elevation Model of the study site

Field reconnaissance is conducted using a handheld GPS (Mapinr v3.8 installed in a smartphone) to select relatively safer areas for establishing the 18 GCPs while maintaining a nearly uniform distribution. To easily detect the GCPs in the acquired images, they are marked with a 60 cm × 60 cm highly reflective material on the ground (Fig. 2) for enhancing the contrast. The coordinates of the centre point of these GCPs are measured in the Vietnam national control network (the VN2000 coordinate system) using the GNSS/RTK method. The base receiver is installed at one control point of the national control network established in the local area. The CHC X91B receivers produced by CHCNAV were used for GNSS measurement. The specification of these receivers is shown in Table 1.

Fig. 2. GCP marks and their coordinates measured by GNSS/RTK

TABLE 1

The specifications of CHC X91B

CHC X91 GNSS Receiver		
	Signal	GPS: L1, L2, L5; GLONASS: L1, L2; BDS: B1, B2, B3; SBAS: WAAS, EGNOS, MSAS
	Kinematic	
	Horizontal:	+ (10 mm + 1 ppm) RMS
	Vertical:	+ (20 mm + 1 ppm) RMS
	Static	
	Horizontal:	+ (5 mm + 1 ppm) RMS
	Vertical:	+(10 mm + 1 ppm) RMS

3. Methodology

3.1. Experiment organisation

To analyse the effect of the number of GCPs and their distribution on the accuracy of a DSM, we tested five different configurations of eight sets of GCP networks, i.e., a total of 40 DSMs are generated. The eight sets of 18 GCPs include networks of 3-15, 4-14, 5-13, 6-12, 7-11, 8-10, 15-3, and 16-2 points, in which the first number represents the number of GCPs used for calibration of the camera-lens model and the second number represents the total number of GCPs used for the assessment of the constructed DSM. The five different configurations for each of the eight cases are depicted in Section 4 (Table 4 and Table 5).

3.2. Software and image processing

The aerial photos collected during the flights are processed using the Agisoft Metashape Professional software (https://www.agisoft.com/). The process includes two main stages, which are block orientation and DSM generation. Since the main objective of this study is to analyse the influence of the number of GCPs on the accuracy of the DSM, all parameters of the processing are kept unchanged. Specifically, both the accuracy of photo alignment and the quality of building dense clouds were set to medium. While the former controlled the accuracy of the camera position estimation, the latter specified the desired reconstruction quality. In addition, the higher the value of the two parameters, the more accurate and comparatively detailed geometry is achieved, but it requires a substantially longer processing time. Although the level of accuracy and detail would reduce with the setting of ‘medium’, it does not make any difference to the effect of GCPs. The processing workflow is shown in Figure 3.

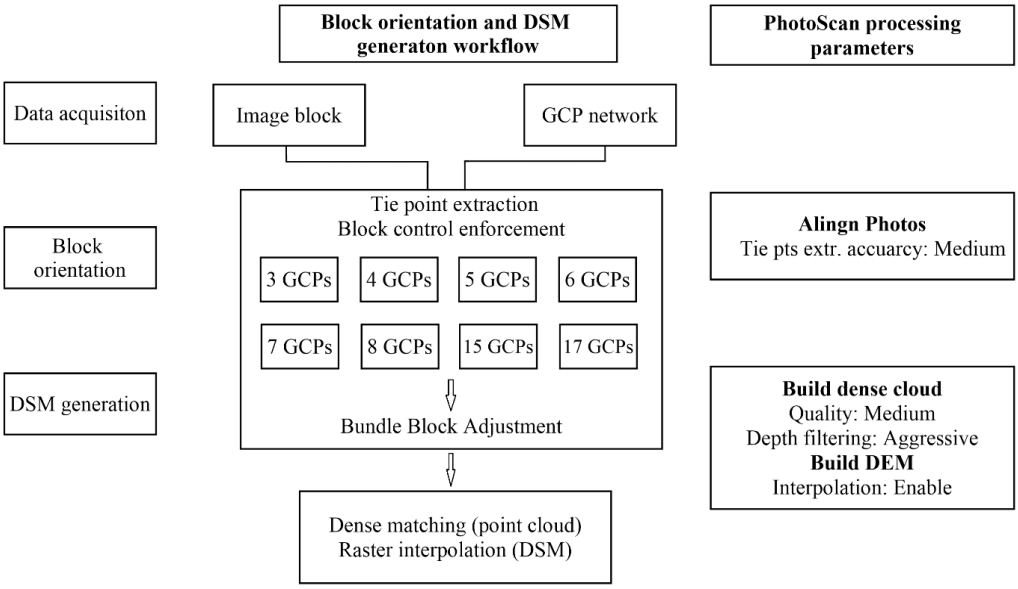

Fig. 3. Data processing workflow for each case of the study by Agisoft Metashape [9]

3.3. Accuracy assessment

The accuracy of the constructed DSMs is assessed using Root Mean Square Error (*RMSE*) in the horizontal ($RMSE_{XY}$) (Eq. (1)), vertical ($RMSE_Z$) (Eq. (2)), and overall components ($RMSE_{XYZ}$) (Eq. (3)), individually for all the 40 DSMs. This is a frequently used method for assessing multiple DSMs in the literature (e.g., [5]). The RMSEs for the three components are computed as:

$$RMSE_{XY} = \sqrt{\left(\frac{1}{n}\right)\sum_{i=1}^{n}\left(X_{DSM} - X_{GCP_i}\right)^2 + \left(Y_{DSM} - Y_{GCP_i}\right)^2} \tag{1}$$

$$RMSE_Z = \sqrt{\left(\frac{1}{n}\right)\sum_{i=1}^{n}\left(Z_{DSM} - Z_{GCP_i}\right)^2} \tag{2}$$

$$RMSE_{XYZ} = \sqrt{\left(\frac{1}{n}\right)\sum_{i=1}^{n}\left(X_{DSM} - X_{GCP_i}\right)^2 + \left(Y_{DSM} - Y_{GCP_i}\right)^2 + \left(Z_{DSM} - Z_{GCP_i}\right)^2} \tag{3}$$

where, n is the total number of checkpoints, (X_{GCP}, Y_{GCP}, Z_{GCP}) and (X_{DSM}, Y_{DSM}, Z_{DSM}) are the 3D coordinates of a given point obtained using GNSS survey and corresponding coordinates on the generated DSM, respectively. Hereafter, this is referred to as inter-case assessment.

An intra-case assessment is also performed for all eight cases. To observe the influence of the different configurations of the same number of GCPs on the DSM generation, i.e.,

the extent and variability of errors, the range of RMSEs in all the components (horizontal, vertical, and overall) for five configurations of the eight cases each are computed using equations (4-6).

$$RMSE_{XY} = RMSE_{XY\_max} - RMSE_{XY\_min} \tag{4}$$

$$RMSE_{Z} = RMSE_{Z\_max} - RMSE_{Z\_min} \tag{5}$$

$$RMSE_{XYZ} = RMSE_{XYZ\_max} - RMSE_{XYZ\_min} \tag{6}$$

4. Results and discussions

The result of the block orientation in terms of camera locations and image residuals are shown in Figures 4a and 4b, respectively. The internal and external orientation parameters of the camera are also determined that comprises 13 parameters. The definition of these 13 parameters is listed in Table 2, while Table 3 depicts their values.

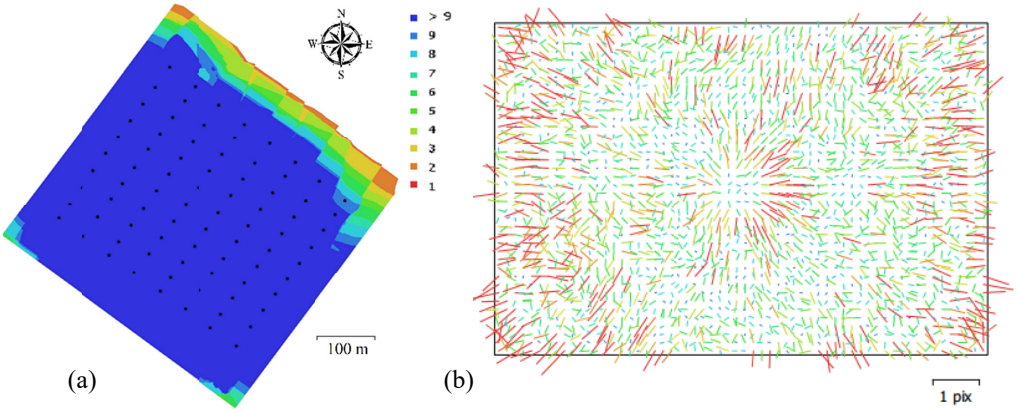

Fig. 4. (a) Camera locations and image overlap; (b) image residuals (for Case 2 and produced by Agisoft Metashape)

TABLE 2

Camera-lens parameters

No	Parameter	Explanation
1	f	Focal length (in pixels)
2	Cx, Cy	Principal point offset of the image in x and y image coordinates (in pixels)
3	B1, B2	Affinity and skew coefficients (in pixels)
4	K1, K2, K3, K4	Radial distortion coefficient of 2nd, 4th, 6th, 8th-order, respectively (dimensionless)
5	P1, P2, P3, P4	Tangential distortion coefficient (dimensionless)

TABLE 3

Camera-lens calibrated coefficient (for Case 2)

No	Parameter	Value	Error
1	f	3870.71	0.38
2	Cx	5.08145	0.019
3	Cy	–1.54674	0.016
4	B1	–12.6349	0.03
5	B2	–17.4018	0.026
6	K1	0.006692	0.000059
7	K2	–0.05837	0.00031
8	K3	0.119846	0.00065
9	K4	–0.08103	0.00047
10	P1	0.000889	1.4E-06
11	P2	–0.0012	9.5E-07
12	P3	0.652888	0.014
13	P4	–0.43653	0.013

The results of the accuracy assessment for cases one and two are depicted in Table 4 and Figure 5, while results for all the other cases are shown in Table 5 and Figure 7. The results in Figure 5 are for the configurations with a minimum $RMSE_{XYZ}$ among all the five configurations for cases one and two. The results in Figure 7 are for the configurations with a maximum $RMSE_{XYZ}$ among all the five configurations for cases three to eight.

TABLE 4

The accuracy of the model in case 1 and case 2

Case 1: (3-15)			
Control points	$RMSE_{XY}$ (m)	$RMSE_{Z}$ (m)	$RMSE_{XYZ}$ (m)
8; 13; 18	0.671	1.874	1.990
8; 13; 21	0.764	2.233	2.360
9; 16; 24	0.673	1.624	1.758
9; 13; 23	0.809	2.204	2.348
12; 17; 20	0.463	1.761	1.821
Case 2: (4-14)			
Control points	$RMSE_{XY}$ (m)	$RMSE_{Z}$ (m)	$RMSE_{XYZ}$ (m)
8; 12; 15; 25	0.174	0.227	0.286
9; 11; 16; 23	0.234	0.390	0.455
9; 13; 16; 24	0.276	0.374	0.465
11; 14; 18; 22	0.298	0.124	0.323
12; 14; 17; 25	0.144	0.135	0.198

From Table 4, the large values of RMSEs for case 1 show that a built model using only 3 GCPs presents a sensitively inferior DSM in terms of reliability. Moreover, the larger range values for case 1 suggest that the accuracy of a DSM is significantly dependent on the configuration if very

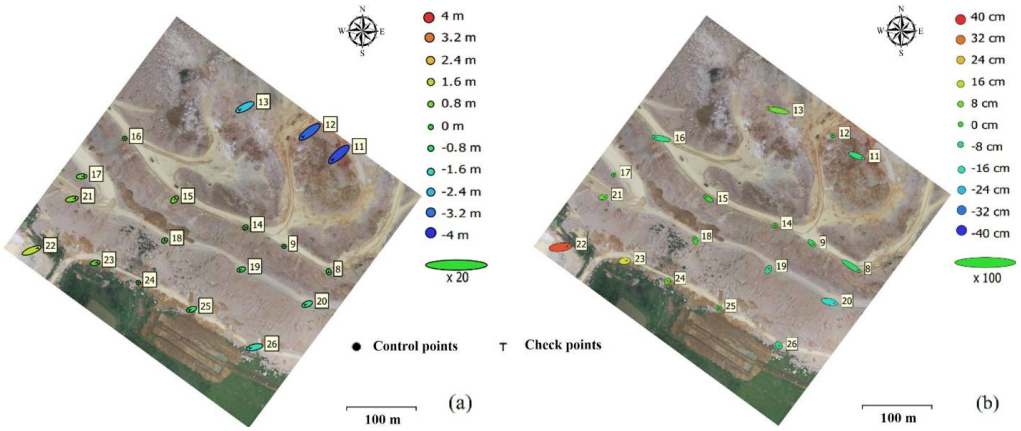

Fig. 5. GCP locations and error estimates (a) – case 1 and (b) – case 2

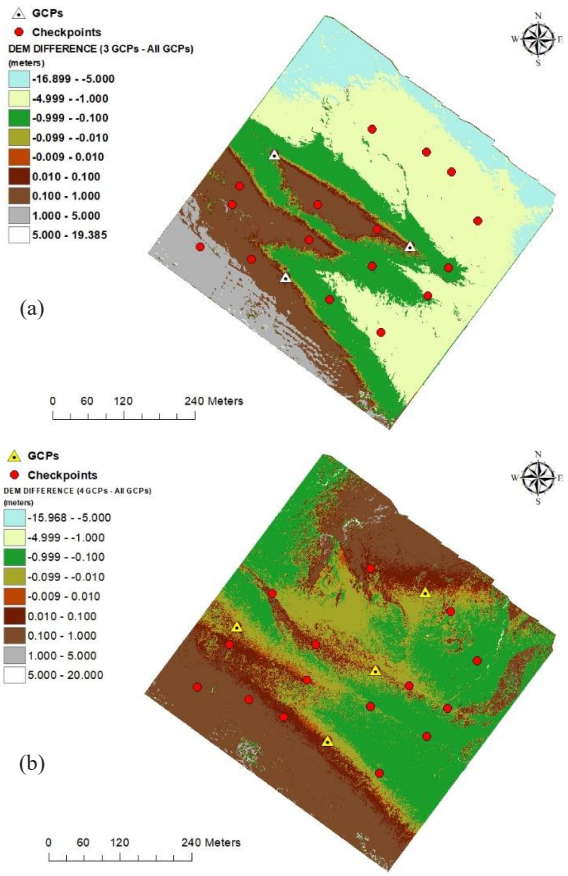

Fig. 6. Differences between DSMs generated in cases of using (a) 3 GCPs; (b) 4 GCPs and all GCPs

TABLE 5

The accuracy of the model in cases 3, 4, 5, 6, 7, and 8

Case 3: (5 control points and 13 checkpoints)			
Control points	$RMSE_{XY}$ (m)	$RMSE_{Z}$ (m)	$RMSE_{XYZ}$ (m)
8-12-15-22-26	0.035	0.048	0.059
8-12-16-23-26	0.034	0.052	0.062
8-13-15-21-25	0.051	0.075	0.090
9-12-15-21-25	0.062	0.078	0.099
9-12-17-23-25	0.051	0.054	0.074
Average	0.047	0.061	0.076
Case 4: (6 control points and 12 checkpoints)			
Control points	$RMSE_{XY}$ (m)	$RMSE_{Z}$ (m)	$RMSE_{XYZ}$ (m)
8-12-14-16-22-26	0.034	0.027	0.043
8-12-16-18-22-26	0.018	0.032	0.037
9-11-13-15-23-25	0.025	0.060	0.065
9-12-15-22-24-26	0.040	0.044	0.059
13-14-16-20-21-25	0.024	0.041	0.047
Average	0.028	0.040	0.050
Case 5: (7 control points and 11 checkpoints)			
Control points	$RMSE_{XY}$ (m)	$RMSE_{Z}$ (m)	$RMSE_{XYZ}$ (m)
8-11-13-16-18-22-26	0.019	0.014	0.024
8-12-15-16-19-21-23	0.019	0.039	0.043
9-12-15-16-21-24-26	0.023	0.033	0.040
11-13-16-19-20-23-25	0.022	0.021	0.030
12-14-15-16-20-23-25	0.029	0.027	0.040
Average	0.022	0.026	0.035
Case 6: (8 control points and 10 checkpoints)			
Control points	$RMSE_{XY}$ (m)	$RMSE_{Z}$ (m)	$RMSE_{XYZ}$ (m)
8-11-13-14-16-18-22-26	0.018	0.022	0.028
8-12-15-16-19-21-23-26	0.026	0.015	0.041
9-11-13-15-16-17-23-26	0.032	0.020	0.038
11-12-14-15-16-20-23-25	0.018	0.027	0.032
11-13-14-16-18-20-22-25	0.020	0.023	0.029
Average	0.023	0.021	0.033
Case 7: (15 control points and 3 checkpoints)			
Checked points	$RMSE_{XY}$ (m)	$RMSE_{Z}$ (m)	$RMSE_{XYZ}$ (m)
9-12-18	0.013	0.009	0.016
11-15-25	0.009	0.020	0.022
13-14-26	0.019	0.024	0.031
14-17-20	0.020	0.019	0.028
16-19-23	0.022	0.026	0.034
Average	0.017	0.019	0.026

TABLE 5. Continued

Case 8: (16 control points and 2 checkpoints)			
Checked points	$RMSE_{XY}$ (m)	$RMSE_{Z}$ (m)	$RMSE_{XYZ}$ (m)
9-21	0.015	0.015	0.022
11-23	0.007	0.028	0.029
16-26	0.018	0.024	0.031
17-20	0.011	0.018	0.022
12-24	0.009	0.019	0.021
Average	0.012	0.020	0.025

few GCPs are used. A drop of maximum $RMSE_{XYZ}$ of 2.36 m for case 1 to a maximum $RMSE_{XYZ}$ of 0.46 m for case 2 is attributable to the addition of one more GCP for DSM construction. The dependence of errors on the configuration can be observed in Table 6, where we have provided the range of RMSEs of the five configurations in all eight cases.

To illustrate the influence of GCPs on the accuracy of DSMs, the pixel-wise difference maps were created (Figs 6a and 6b) between the pairs of DSMs from cases 1 and 2, and an ideal case using all 18 GCPs. Figures 6a and 6b suggest that the uniform distribution of the GCPs should not be done only in the horizontal plane, but the vertical uniformity is also required for GCPs placement. If the GCPs are only in low-lying areas, then the accuracy cannot be expected/obtained in the high-lying areas and vice-versa. Hence, the vertical distribution must be strictly followed for a high-undulating terrain like open-pit mines, where we have a large range of heights. The effect of considering the vertical distribution is exemplified in Figure 6a versus 6b. Furthermore, the relatively lower error in interpolation compared to larger errors in extrapolation is also observed in Figures 6a and 6b.

Though an idea of the increase in accuracy by increasing GCPs is depicted from cases 1 and 2 in Table 4, we do not recommend the use of either three or four GCPs for DSM generation. This is because they do not meet the accuracy required for a mining project and more importantly, with the use of fewer GCPs, the DSM accuracy is highly susceptible to the different configurations of the GCPs, even if they are distributed uniformly (Tables 4 and 6). Hence, DSMs generated using very few GCPs are uncertain and inconsistent.

From Table 5 and Table 6, the same observations are found for other cases, i.e., with the increase in the number of GCPs, i) the accuracy of a DSM improves, and ii) the dependency on the configuration of GCPs decreases. The minimum *RMSEXYZ* for case 3 and case 8 are 0.059 m and 0.021 m, respectively. It is observed from Table 5 that the average *RMS EXY* and average *RMS EZ* are improved from 0.047 m and 0.061 m for case 3 to 0.012 m and 0.020 m for case 8, respectively. From Tables 4-6, a substantial improvement is observed in the accuracy of a DSM with an increase in the number of GCPs from 3 to 5. Comparatively less significant improvement occurred when number of GCPs were increased from 5 to 6 and further to 7. Although case 3 with 5 GCPs is sufficient for our purpose, an improvement of 2 cm in the height accuracy is observed with 6 GCPs. Therefore, we suggest using 6 GCPs for a DSM generation of small to medium-sized open-pit mines, with areas up to 36 hectares with some cautions on the configuration. However, as a factor of safety, 7 GCPs is highly recommended as it has sub-centimetre dependency on the network configuration. It should be noted that the condition of uniform distribution is still applicable.

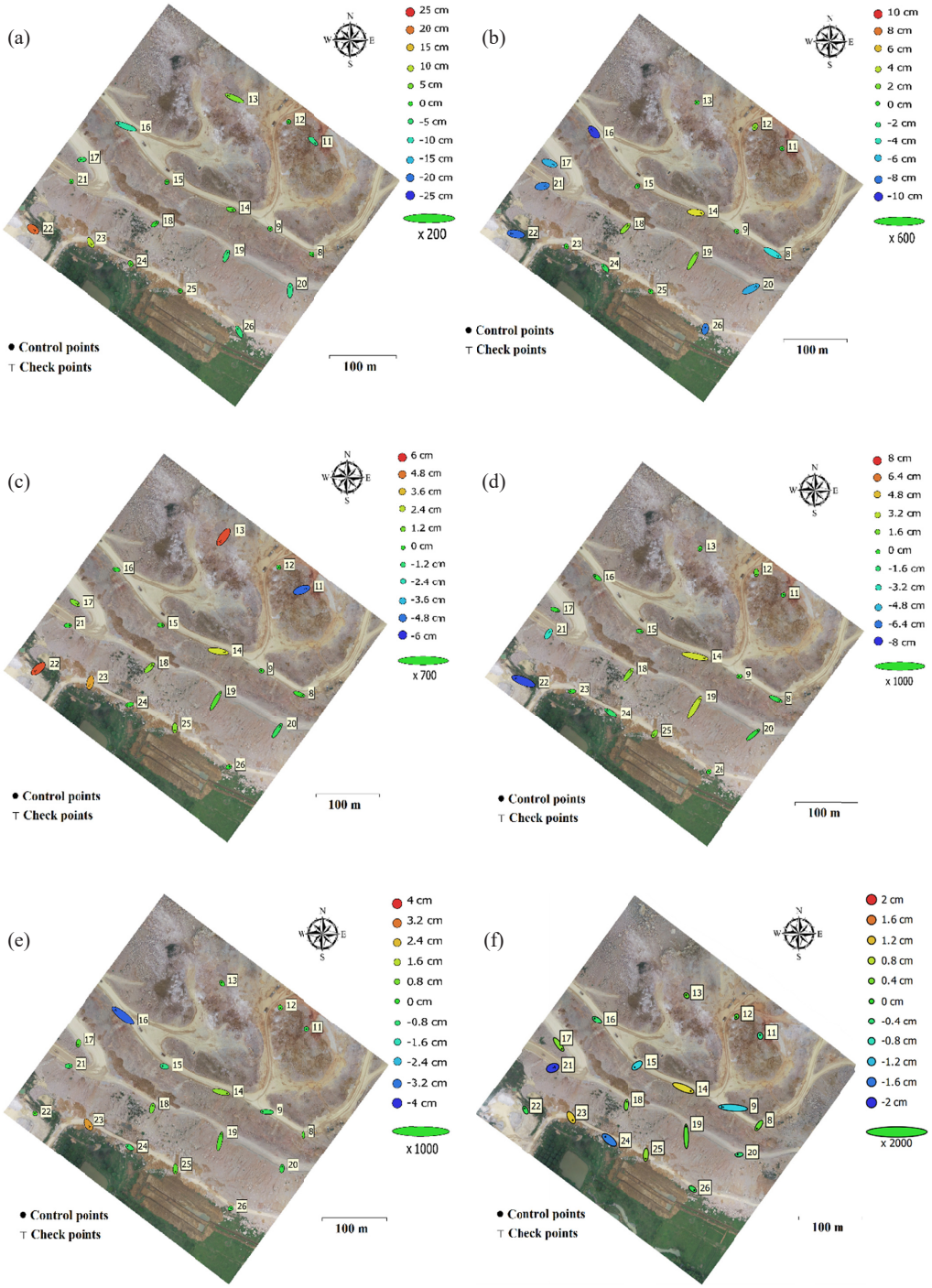

Fig. 7. GCP locations and error estimates (a) case 3, (b) case 4, (c) case 5, (d) case 6, (e) case 7, and (f) case 8

The colour of the error ellipses in Figure 5 and Figure 7 indicates the error in the Z component of the GCPs, while the ellipse shape represents the error in the X and Y components. Table 6 represents the difference between the maximum and minimum RMSEs of five configurations for all eight cases, hence depicting the spread of the error for different configurations of a given number of GCPs.

TABLE 6

Differences between the max and min *RMSE*s in five configurations for all the eight cases

Case	$\Delta RMSE_{XY}$ (m)	$\Delta RMSE_{Z}$ (m)	$\Delta RMSE_{XYZ}$ (m)
1	0.346	0.609	0.602
2	0.154	0.266	0.267
3	0.028	0.030	0.040
4	0.022	0.033	0.028
5	0.010	0.025	0.019
6	0.014	0.012	0.013
7	0.013	0.017	0.018
8	0.011	0.013	0.010

5. Conclusion

In this study, a detailed investigation has been conducted on the influence of the number of GCPs, and their network configurations on the quality of DSM generated using the UAV-based method over small quarries. A lightweight DJI Phantom 4 Pro UAV was used to generate 40 DSMs of the Long Son quarry in Thanh Hoa province, Vietnam. The analysis was carried out on five configurations of each of the eight combinations of 18 GCPs, for DSM generation and accuracy assessment.

It is concluded from experiments that an increase in the number of GCPs results in an improvement in the accuracy of DSMs and decreases the dependency on the network configuration of the GCPs. However, a precise DSM is required at regular intervals of time in a mining project for various applications. Therefore, we tried to find an optimal solution for small to medium-sized open-pit mines that involved finding the optimal number of GCPs to obtain sufficiently accurate DSMs while maintaining safety, time, and cost-effectiveness. The results showed that to achieve an average accuracy well within 10 cm, five GCPs are sufficient and six GCPs to obtain the accuracy up to 5 cm. However, we strongly recommend using seven GCPs as it provides an average overall accuracy within 3.5 cm, with vertical accuracy being 2.6 cm. Moreover, with a $\Delta RMSE$ of all the components within 1.8 cm, it is concluded that using seven GCPs decreases the dependency on network configuration. Notably, the condition of uniform distribution of the GCPs must be maintained.

We acknowledge that the accuracy of DSM will also be dependent on the flight height of UAVs. However, this was not included in our analysis. This study tried to fill a possible literature gap on the influence of the number of GCPs on DSM generation of the small to medium-sized open-pit mines using lightweight UAVs. Our results from open-pit mines suggest that a UAV-based survey is a useful and efficient approach for mapping in the rugged topographies, and thus, further applications in the mining industry.

Acknowledgements

This work was financially supported by the Ministry of Education and Training (MOET) in Vietnam under grant number B2020-MDA-14.

Data Availability Statement

Some or all data, models, or codes that support the findings of this study are available from the corresponding authors upon reasonable request.

Conflicts of Interest

The authors declare no conflict of interest.

References

[1] B. Kršák, P. Blišťan, A. Pauliková, P. Puškárová, Ľ. Kovanič, J. Palková, V. Zelizňaková, Use of low-cost UAV photogrammetry to analyze the accuracy of a digital elevation model in a case study. Measurement **91**, 276-287 (2016). DOI: https://doi.org/10.1016/j.measurement.2016.05.028

[2] C. Cryderman, S.B. Mah, A. Shufletoski, Evaluation of UAV Photogrammetric Accuracy for Mapping and Earthworks Computations. GEOMATICA **68**, 309-317 (2014). DOI: https://doi.org/10.5623/cig2014-405

[3] C. Hugenholtz, O. Brown, J. Walker, T. Barchyn, P. Nesbit, M. Kucharvzyk, S. Myshak, Spatial accuracy of UAV-derived orthoimagery and topography: comparing photogrammetric models processed with direct geo-referencing and ground control points. GEOMATICA **70**, 21-30 (2016). DOI: https://doi.org/10.5623/cig2016-102

[4] D. Tien Bui, N.Q. Long, X.-N. Bui, V.-N. Nguyen, C. Van Pham, C. Van Le, P.-T.T. Ngo, D. Tien Bui, B. Kristoffersen, Lightweight Unmanned Aerial Vehicle and Structure-from-Motion Photogrammetry for Generating Digital Surface Model for Open-Pit Coal Mine Area and Its Accuracy Assessment, in: D. Tien Bui, A. Ngoc Do, H.-B. Bui, N.-D. Hoang, (eds.), Advances and Applications in Geospatial Technology and Earth Resources, Springer International Publishing, Cham, 17-33 (2018). DOI: https://doi.org/10.1007/978-3-319-68240-2_2

[5] F. Agüera-Vega, F. Carvajal-Ramírez, P. Martínez-Carricondo, Accuracy of Digital Surface Models and Orthophotos Derived from Unmanned Aerial Vehicle Photogrammetry. J. Surv. Eng. **143**, 04016025 (2017). DOI: https://doi.org/10.1061/(ASCE)SU.1943-5428.0000206

[6] F. Beretta, H. Shibata, R. Cordova, R. de L. Peroni, J. Azambuja, J.F.C.L. Costa, Topographic modelling using UAVs compared with traditional survey methods in mining. REM, Int. Eng. J. **71**, 463-470 (2018). DOI: https://doi.org/10.1590/0370-44672017710074

[7] F. Mancini, M. Dubbini, M. Gattelli, F. Stecchi, S. Fabbri, G. Gabbianelli, Using Unmanned Aerial Vehicles (UAV) for High-Resolution Reconstruction of Topography: The Structure from Motion Approach on Coastal Environments. Remote Sensing **5**, 6880-6898 (2013). DOI: https://doi.org/10.3390/rs5126880

[8] G. Esposito, G. Mastrorocco, R. Salvini, M. Oliveti, P. Starita, Application of UAV photogrammetry for the multi-temporal estimation of surface extent and volumetric excavation in the Sa Pigada Bianca open-pit mine, Sardinia, Italy. Environ. Earth Sci. **76**, 103 (2017). DOI: https://doi.org/10.1007/s12665-017-6409-z

[9] G. Forlani, E. Dall'Asta, F. Diotri, U.M. di Cella, R. Roncella, M. Santise, Quality assessment of DSMs produced from UAV flights geo-referenced with onboard RTK positioning. Remote Sensing **10**, 311 (2018). DOI: https://doi.org/10.3390/rs10020311

[10] J. Fernández-Lozano, A. González-Díez, G. Gutiérrez-Alonso, R. Carrasco, J. Pedraza, J. García-Talegón, G. Alonso-Gavilán, J. Remondo, J. Bonachea, M. Morellón, New perspectives for UAV-based modelling the Roman gold mining infrastructure in NW Spain. Minerals **8**, 518 (2018). DOI: https://doi.org/10.3390/min8110518

[11] J. Malos, B. Beamish, L. Munday, P. Reid, C. James, Remote monitoring of subsurface heatings in opencut coal mines, in: N. Aziz and B. Kininmonth (eds.), Proceedings of the 2013 Coal Operators' Conference, Mining Engineering, University of Wollongong (2013).

[12] J.-C. Padró, V. Carabassa, J. Balagué, L. Brotons, J.M. Alcañiz, X. Pons, Monitoring opencast mine restorations using Unmanned Aerial System (UAS) imagery. Sci. Total Environ. **657**, 1602-1614 (2019). DOI: https://doi.org/10.1016/j.scitotenv.2018.12.156

[13] J.K.S. Villanueva, A.C. Blanco, Optimization of ground control point (GCP) configuration for unmanned aerial vehicle (UAV) survey using structure from motion (SfM). Int. Arch. Photogramm. Remote Sens. Spatial Inf. Sci. **XLII-4/W12**, 167-174 (2019). DOI: https://doi.org/10.5194/isprs-archives-XLII-4-W12-167-2019

[14] J.M.G. Rangel, G.R. Gonçalves, J.A. Pérez, The impact of number and spatial distribution of GCPs on the positional accuracy of geospatial products derived from low-cost UASs. Int. J. Remote Sens. **39**, 7154-7171 (2018). DOI: https://doi.org/10.1080/01431161.2018.1515508

[15] K. Szentpeteri, T.R. Setiawan, A. Ismanto, Drones (UAVs) in mining and Exploration. An application example: pit mapping and geological modelling, in: Unconventional Exploration Target & Latest Technique and New Tools in Mineral and Coal Exploration, (2016).

[16] K.N. Tahar, An evaluation on different number of ground control points in unmanned aerial vehicle photogrammetric block, Int. Arch. Photogramm. Remote Sens. Spatial Inf. Sci. **XL-2/W2**, 93-98 (2013). DOI: https://doi.org/10.5194/isprsarchives-XL-2-W2-93-2013

[17] L. Ge, X. Li, A.H.-M. Ng, UAV for mining applications: A case study at an open-cut mine and a longwall mine in New South Wales, Australia, in: IEEE International Geoscience and Remote Sensing Symposium (IGARSS), 2016, 5422-5425 (2016). DOI: https://doi.org/10.1109/IGARSS.2016.7730412

[18] Ľ. Kovanič, P. Blišťan, V. Zelizňaková, J. Palková, Surveying of open pit mine using low-cost aerial photogrammetry, in I. Ivan, A. Singleton, J. Horák, T. Inspektor (Eds.), The Rise of Big Spatial Data. Springer International Publishing, Cham (2017). DOI: https://doi.org/10.1007/978-3-319-45123-7_9

[19] L. Van Canh, C. Xuan Cuong, N. Quoc Long, L. Thi Thu Ha, T. Trung Anh, X.-N. Bui, Experimental Investigation on the Performance of DJI Phantom 4 RTK in the PPK Mode for 3D Mapping Open-Pit Mines. Inżynieria Mineralna **1**, 65-74 (2020). DOI: https://doi.org/10.29227/IM-2020-02-10

[20] M. Alvarado, F. Gonzalez, A. Fletcher, A. Doshi, Towards the development of a low cost airborne sensing system to monitor dust particles after blasting at open-pit mine sites. Sensors **15**, 19667-19687 (2015). DOI: https://doi.org/10.3390/s150819667

[21] M. Francioni, R. Salvini, D. Stead, R. Giovannini, S. Riccucci, C. Vanneschi, D. Gullì, An integrated remote sensing-GIS approach for the analysis of an open pit in the Carrara marble district, Italy: Slope stability assessment through kinematic and numerical methods. Comput. Geotech. **67**, 46-63 (2015). DOI: https://doi.org/10.1016/j.compgeo.2015.02.009

[22] M. Shahbazi, G. Sohn, J. Théau, P. Menard, Development and Evaluation of a UAV-Photogrammetry System for Precise 3D Environmental Modeling. Sensors **15**, 27493-27524 (2015). DOI: https://doi.org/10.3390/s151127493

[23] M.R. James, S. Robson, M.W. Smith, 3-D uncertainty-based topographic change detection with structure-from-motion photogrammetry: precision maps for ground control and directly georeferenced surveys. Earth Surf. Process. Landforms **42**, 1769-1788 (2017). DOI: https://doi.org/10.1002/esp.4125

[24] M.R. James, S. Robson, S. d'Oleire-Oltmanns, U. Niethammer, Optimising UAV topographic surveys processed with structure-from-motion: Ground control quality, quantity and bundle adjustment. Geomorphology **280**, 51-66 (2017). DOI: https://doi.org/10.1016/j.geomorph.2016.11.021

[25] N.Q. Long, B.X. Nam, C.X. Cuong, L.V. Canh, An approach of mapping quarries in Vietnam using low-cost Unmanned Aerial Vehicles. Inżynieria Mineralna **11**, 248-262 (2019). DOI: https://doi.org/10.29227/IM-2019-02-79

[26] O. Mian, J. Lutes, G. Lipa, J.J. Hutton, E. Gavelle, S. Borghini, Direct georeferencing on small unmanned aerial platforms for improved reliability and accuracy of mapping without the need for ground control points. Int. Arch. Photogramm. Remote Sens. Spatial Inf. Sci. **XL-1/W4**, 397-402 (2015). DOI: https://doi.org/10.5194/isprsarchives-XL-1-W4-397-2015

[27] P.L. Raeva, S.L. Filipova, D.G. Filipov, Volume computation of a stockpile-a study case comparing GPS and UAV measurements in an open pit quarry. Int. Arch. Photogramm. Remote Sens. Spatial Inf. Sci. **XLI-B1**, 999-1004 (2016). DOI: https://doi.org/10.5194/isprsarchives-XLI-B1-999-2016

[28] S. Coveney, K. Roberts, Lightweight UAV digital elevation models and orthoimagery for environmental applications: data accuracy evaluation and potential for river flood risk modelling. Int. J. Remote Sens. **38**, 3159-3180 (2017). DOI: https://doi.org/10.1080/01431161.2017.1292074

[29] T. Tonkin, N. Midgley, Ground-Control Networks for Image Based Surface Reconstruction: An Investigation of Optimum Survey Designs Using UAV Derived Imagery and Structure-from-Motion Photogrammetry. Remote Sensing **8**, 786 (2016). DOI: https://doi.org/10.3390/rs8090786

[30] Z. Ren, J. Tang, T. Kalscheuer, H. Maurer, Fast 3-D large-scale gravity and magnetic modeling using unstructured grids and an adaptive multilevel fast multipole method. J. Geophys. Res. Solid Earth **122**, 79-109 (2017). DOI: https://doi.org/10.1002/2016JB012987